High-resolution powder neutron diffraction study of helimagnetic order in $CrP_{1-x}V_xO_4$ solid solutions

J. P. Wright and J. P. Attfield
Department of Chemistry, University of Cambridge, Lensfield Road, Cambridge CB2 1EW, United Kingdom

W. I. F. David
ISIS Facility, Rutherford Appleton Laboratory, Chilton OX11 0QX, United Kingdom

J. B. Forsyth
Clarendon Laboratory, University of Oxford, Parks Road, Oxford OX1 3PU, United Kingdom

(Received 7 January 2000)

High-resolution powder neutron diffraction measurements on $CrP_{1-x}V_xO_4$ samples with $x=0$, 0.02, 0.04, 0.06 and 0.08 have yielded precise parameters for their low temperature helimagnetic structures which have a magnetic propagation vector $(k_x,0,0)$. The refined values of k_x increase from $k_x=0.331$ for $x=0$ to $k_x=0.337$ for $x=0.08$ and no tendency of the incommensurate spiral to ''lock-in'' to the commensurate periodicity $k_x=1/3$ is observed. The ordered Cr^{3+} magnetic moment decreases from $2.32(3)\mu_B$ to $1.72(6)\mu_B$ for $x=0$ to $x=0.08$. Field and zero-field cooled magnetic susceptibility measurements evidence increasing static magnetic disorder with x, in agreement with the neutron-diffraction results.

1. INTRODUCTION

Superexchange interactions and single ion anisotropy are important in determining the magnetic ordering in oxosalts with the β-$CrPO_4$ type crystal structure. Spiral magnetic structures can arise when the superexchange interactions in the material are frustrated and are dominant over the single ion anisotropy. In some cases this balance of exchange interactions is determined by symmetry, however, in these orthorhombic crystal structures, the frustration arises through coincidence. The crystal and magnetic structure[1] of β-$CrPO_4$ is shown on Fig. 1. The crystal structure has Cmcm space-group symmetry. Chains of edge sharing CrO_6 octahedra run parallel to the c axis separated by tetrahedral phosphate groups and the magnetic moments are coupled antiferromagnetically along the chains of octahedra. The magnetic structure at 5 K was previously found to be a cycloidal spiral of moments which propagates along [100] with a periodicity of $3.07(3)a_0$, where a_0 is the cell parameter. The Neél temperature was identified as $\sim$23 K from a variable temperature neutron diffraction study.[2] Magnetic frustration between the chains of octahedra leads to the formation of the spiral magnetic structure. $MnSO_4$ has an analogous crystal and magnetic structure[3] to β-$CrPO_4$ although in that case a cone component of the spiral is observed and the periodicity of the spiral is $\sim 6a_0$. A theoretical analysis by Solyom indicates the magnetic structure in $MnSO_4$ should arise through three separate phase transitions[4] and this has been born out by experiments.[5] $CrVO_4$ is also isostructural with β-$CrPO_4$ but has a collinear antiferromagnetic structure[6] in which the intrachain order is again antiferromagnetic, but the interchain order is ferromagnetic.

$CoSO_4$ is isostructural with β-$CrPO_4$ and has a magnetic structure which is strongly influenced by single ion anisotropy. The moments form a simple commensurate structure with two antiferromagnetic sublattices having the moments tilted $\pm 25°$ from the crystallographic b axis.

The moment directions are determined by the strong single-ion anisotropy of Co^{2+}. In VPO_4 (another β-$CrPO_4$ type material) the interplay between single-ion anisotropy and superexchange is clearly demonstrated by the temperature dependence of the magnetic structures. An incommensurate structure was found at 11.7 K where the periodicity of the spiral is $1.78a_0$ at 23.4 K.[7] It gradually increases to $2a_0$ at 10.3(5) K below which the structure is locked into this commensurate configuration. These different magnetic structures reflect the varying balance of interchain superexchange interactions. Other examples where single-ion anisotropy locks the propagation vector into a commensurate configuration have been observed in spin slip systems. For example, in metallic holmium[8] a series of commensurate configurations are observed as a function of temperature and magnetic field.

The use of high-resolution time of flight neutron powder

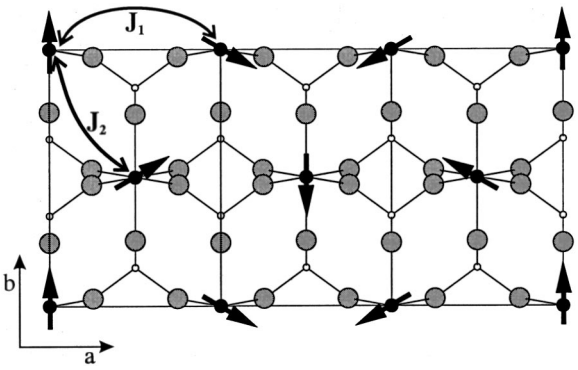

FIG. 1. Crystal and magnetic structure of β-$CrPO_4$ in the $z=0$ plane. Cr^{3+} ions at height $z=1/2$ have opposite moments to those pictured, giving antiferromagnetic order out of the plane. Open circles—P, grey circles—O, filled circles—Cr.

diffraction allows complex magnetic structures to be examined in great detail. Propagation vectors describing incommensurate magnetic structures can be determined with a precision of ~0.01%.[9] Since the $3d^3$:$^4A_{1g}$ Cr^{3+} ion in β-$CrPO_4$ has no orbital contribution to the magnetic moment, the single-ion anisotropy is expected to be small compared to that in $CoSO_4$ and VPO_4. However, the previously determined propagation vector is close to a commensurate configuration, suggesting that the structure may be locked in to a $3\times1\times1$ magnetic supercell. The purpose of this investigation is to determine whether β-$CrPO_4$ is locked into a commensurate $k_x=1/3$ configuration by local anisotropic interactions. The similarity of the structures of β-$CrPO_4$ and $CrVO_4$ suggested the possibility of preparing solid solutions in which the superexchange interactions will be altered, while retaining similar single-ion anisotropies.

2. EXPERIMENTAL

The preparation of the undoped sample has been described previously[1] and doped samples were prepared using an analogous method. Appropriate stoichiometric quantities of $Cr(NO_3)_3.9H_2O$, $NH_4H_2PO_4$ and NH_4VO_3 were dissolved in $HNO_3(aq)$ (~2 M) and the solution was boiled to dryness. The residue was carefully heated using a Bunsen burner until no more gases were evolved and then ground and placed in an alumina boat. The $x=0.02$, 0.04, and 0.06 samples were then heated to 1000 °C and the 0.08 sample to 900 °C. Samples with higher vanadate compositions were also synthesized although it was not possible to obtain these as phase pure products. X-ray powder diffraction measurements were carried out using a Philips PW1710 diffractometer which confirmed the formation of a single phase solid solution. Heating to higher temperatures led to the formation of an α-$CrPO_4$ type phase[10] and this phase was also found in samples prepared with higher than 8% vanadate content. Rietveld fits to the x-ray powder data of the solid solutions were performed using the GSAS (Ref. 11) program to extract the cell parameters. A Quantum Design superconducting quantum interference device (SQUID) magnetometer was used for susceptibility measurements between 4 K and 250 K for the $x=0.02$ and 0.08 samples in a field of 2 kOe. Further measurements were carried out for the $x=0$ and 0.08 samples with the sample cooled in zero field, and in the measuring field of 100 Oe, between 6 and 60 K.

Neutron powder diffraction measurements were carried out using the HRPD instrument at the ISIS facility, using both the detector banks in backscattering geometry and at $2\theta=90°$. For the undoped sample a pulse repetition rate of 10 Hz was used with a time-of-flight (TOF) range of 70–170 ms at sample temperatures of 2 K, 10 K, 17 K, and 30 K. Further data were obtained with a TOF range of 30–130 ms at 2 K and 30 K to give a greater range of data for refinement of the crystallographic structure. Data were collected at 2 K for $x=0.04$ and at 2 K and 30 K for $x=0.02$, 0.06, and 0.08 with a neutron pulse repetition rate of 5 Hz and a TOF range of 35–235 ms. The data were normalized to the incident beam intensity and corrected for detector efficiency. Rietveld refinements of the magnetic structure were carried out using the program TF112M (Ref. 12) with the data from the 90° bank. This program allows for the refinement of spiral magnetic structures from single histograms of TOF data together with the usual crystallographic parameters. The crystal structures were refined from the backscattering data using the GSAS computer program which provided a better model for the anisotropic peak shape effects.

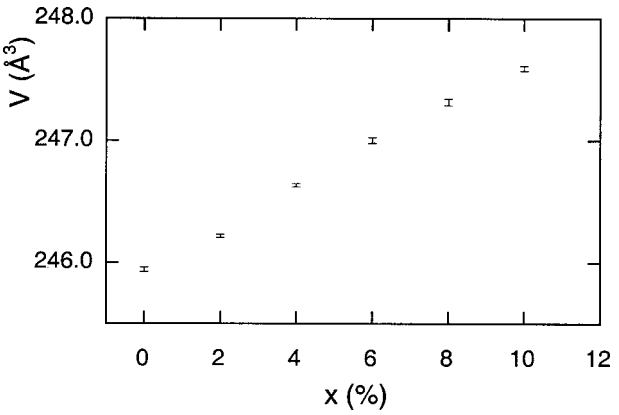

FIG. 2. Variation of refined unit-cell volume with vanadate content for $CrP_{1-x}V_xO_4$ solid solutions from 300 K x-ray diffraction data.

3. POWDER DIFFRACTION RESULTS

The x-ray diffraction patterns of the $CrP_{1-x}V_xO_4$ solid solutions showed peak shifts which were dependent upon x, indicating the formation of a solid solution. Figure 2 shows the variation of the unit-cell volume with doping, which follows Vegard's law up to $x\approx0.10$. However, ~1% (by mass) of Cr_2O_3 was observed in the neutron diffraction patterns for all the samples and a small amount (<1%) of α-$CrPO_4$ (Ref. 10) was observed in the $x=0.06$ sample. Samples with vanadate contents greater than $x=0.08$ could not be prepared without significant fractions of the α-$CrPO_4$ phase, indicating that the substitution stabilizes the latter structure type over the β-$CrPO_4$ phase.

Each HRPD experiment provides a high-resolution diffraction profile from the backscattering counter bank and a profile of a lower resolution from the 90° counter bank. Initial comparisons of independently refined values of the k_x propagation vector component using each profile showed that the value and estimated standard deviation (esd) were essentially the same for both banks. The peak shape was not well described for the backscattering data using a standard peak function with the full width at half maximum (FWHM) varying only as a function of TOF. This accounts for the similarity of the precision of the refined parameters. Further investigations showed that there was an *hkl*-dependent asymmetric peak broadening effect in the backscattering data which complicated the analysis. The effect increased with x but was also evident in the undoped sample. Figure 3 shows a small range of the backscattering data where the peak broadening effects are particularly clear. These effects were present in the nuclear diffraction peaks data from both above and below the magnetic ordering temperature indicating that they are inherent to the crystal structures.

The 90° bank data were used for refinements of the magnetic structure because of the peak broadening effects. To test for any systematic errors in the refinement of k_x, refine-

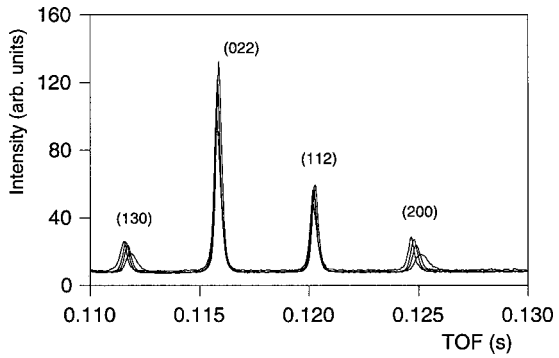

FIG. 3. Anisotropic and asymmetric peak broadening effects in the high-resolution backscattering datasets for $CrP_{1-x}V_xO_4$. Peaks move to higher TOF as x increases from 0 to 0.08.

ments with the majority of the broadened peaks excluded were compared to those with narrow peaks excluded. No systematic errors were detected in this way. Rietveld refinements in Fig. 4 compare fits with k_x constrained as $k_x=1/3$ and refined as a free parameter for the $x=0$ sample. The dependence of the propagation vector and ordered magnetic moment upon vanadate substitution is shown on Figs. 5 and 6. For the $x=0$ sample, the refined value of the ordered moment at 2 K of $2.36(3)\mu_B$ is slightly lower than the value of $2.55(10)\mu_B$ obtained previously[1] at 5 K. The moment decreases to $2.26(3)\mu_B$ at 10 K and further to $1.90(3)\mu_B$ at 17 K. The refined values of k_x at 10 K and 17 K were 0.3305(2) and 0.3307(3), respectively, and show no significant change from the value of $k_x=0.3306(2)$ at 2 K.

The backscattering neutron diffraction data of the $CrP_{1-x}V_xO_4$ solid solutions showed anisotropic and asymmetric peak broadening effects which could not be fitted by a standard TOF peak shape, and so a function consisting of a pair of back-to-back exponentials convoluted with a pseudo-Voight function was used.[11] Although the *hkl* dependence of various aspects of the peak shape were measured, a consistent model for the observed effects could not be deduced from these data alone. To obtain consistent refinements of the crystal structures from the backscattering profiles, a limited range of data common to all samples (42–100 ms,

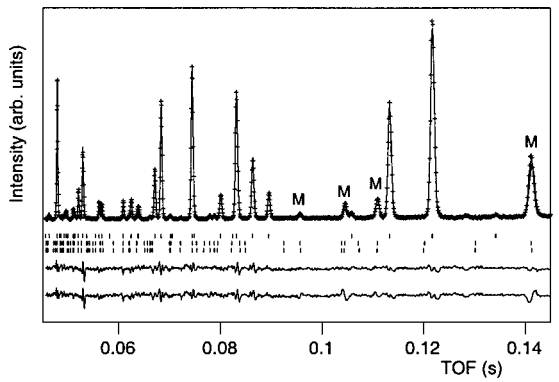

FIG. 4. Observed (crosses), calculated and difference/esd curves for β-$CrPO_4$ at 2 K, refined using TF112M and data from the 90° HRPD data bank. The upper difference curve is for k_x refined, and the lower is with k_x fixed at 1/3. The upper Bragg reflection markers indicate structural peaks, the middle row is for k_x refined and lower row for $k_x=1/3$. Prominent magnetic peaks are marked *M*.

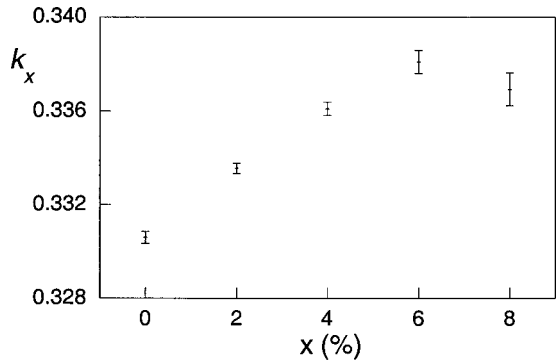

FIG. 5. Refined propagation vector versus vanadate content in $CrP_{1-x}V_xO_4$.

equivalent to a *d*-spacing range of 0.89 Å to 2.07 Å) was used. This excludes the extreme peak shape mismatches that are evident at longer TOF's. Much improved fits were obtained by taking into account symmetric anisotropic peak broadening effects. An empirical strain based algorithm[13] was used where the strain matrix L_{ij} is included as follows:

$$L_{hkl}=(L_{11}h^2+L_{22}k^2+L_{33}l^2+2L_{12}hk+2L_{23}kl+2L_{13}hl)d_{hkl}^3,$$

where h, k and l are the conventional Miller indices, d_{hkl} is the d spacing for the peak, L_{ij} are refineable parameters, and L_{hkl} is the FWHM of the Lorentzian component of the peak shape. Although this accounts for an *hkl* dependence of the peak broadening, it is not completely satisfactory as the peak broadening is modeled symmetrically, although some asymmetry is present in the observed broadening. The refinements became progressively worse with higher vanadate content as the asymmetry of the peak broadening increased. The broadest peaks are those that are shifted most by the vanadate substitution, suggesting that x has a nonrandom distribution throughout the sample.

In spite of the difficulties in modeling the peak shape for these very highly resolved data, good refinements were obtained using the backscattering profiles, the results of which are summarized in Table I. A typical fit is shown in Fig. 7 and selected bond distances and bond angles are summarized in Table II.

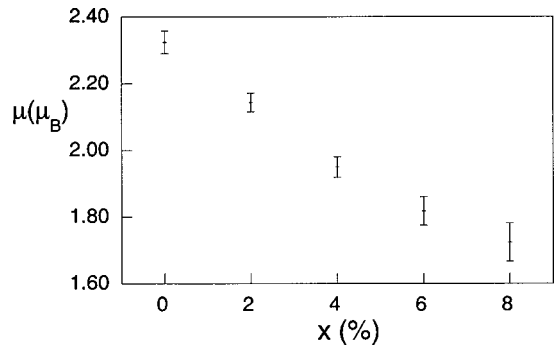

FIG. 6. Refined magnetic moment versus vanadate content in $CrP_{1-x}V_xO_4$.

TABLE I. Agreement factors and refined atomic coordinates,[a] cell and peak shape parameters for $CrP_{1-x}V_xO_4$ samples at 4 K from fits to the HRPD backscattering data.

x	0.00	0.02	0.04	0.06	0.08
χ^2	6.57	3.80	4.64	5.87	13.3
R_{wp}(%)	3.77	3.26	3.32	3.94	5.20
R_p(%)	2.92	2.60	2.64	2.92	3.80
Py	0.3502(2)	0.3501(2)	0.3498(2)	0.3494(3)	0.3494(3)
O(1)y	0.2460(1)	0.2455(2)	0.2457(2)	0.2458(2)	0.2458(2)
O(1)z	0.0427(1)	0.0426(2)	0.0424(2)	0.0421(2)	0.0417(2)
O(2)x	0.2455(2)	0.2459(2)	0.2463(2)	0.2463(4)	0.2469(4)
O(2)y	0.4700(1)	0.4703(1)	0.4703(1)	0.4702(2)	0.4704(2)
U_{iso}/Å^2	0.0002(6)	0.0018(7)	0.0037(7)	0.004(1)	0.006(1)
a/Å	5.16774(4)	5.17381(4)	5.17888(5)	5.18398(9)	5.18996(1)
b/Å	7.75233(6)	7.76119(6)	7.76700(7)	7.77198(12)	7.77886(15)
c/Å	6.11363(6)	6.11206(5)	6.11073(5)	6.11075(9)	6.10878(9)
Vol/Å^3	244.925(2)	245.429(2)	245.800(2)	246.201(5)	246.624(5)
σ_1/μ sec Å^{-1}	1750(30)	1630(30)	1850(40)	2570(90)	2940(90)
L_{11}/μ sec Å^{-1}	1.54(5)	1.91(5)	2.69(6)	5.10(13)	6.00(15)
L_{22}/μ sec Å^{-1}	1.22(3)	1.01(3)	1.11(3)	1.72(5)	1.95(6)
L_{33}/μ sec Å^{-1}	3.13(5)	2.02(5)	1.51(4)	2.08(8)	1.21(7)
L_{12}/μ sec Å^{-1}	0.32(4)	0.17(4)	0.27(4)	0.46(7)	0.79(8)
L_{13}/μ sec Å^{-1}	−0.79(4)	−0.59(4)	−0.76(4)	−1.30(8)	−1.59(9)
L_{23}/μ sec Å^{-1}	−0.69(4)	−0.39(4)	−0.42(4)	−0.66(10)	−0.89(7)

[a]Full coordinates in space group Cmcm are Cr in 4(a) (0, 0, 0); P in 4(c) (0, y, 1/4); O(1) in 8(f) (0, y, z); O(2) in 8(g) (x, y, 1/4).

4. MAGNETIC SUSCEPTIBILITY RESULTS

The inverse susceptibility versus temperature data for the $x=0.02$ and 0.08 samples together with Curie Weiss fits are shown on Fig. 8. We obtain values of $3.82(1)\mu_B$ and $3.81(1)\mu_B$ for the paramagnetic moment, respectively, in good agreement with the spin-only value of $3.89\mu_B$. The Weiss constants for the 0.02 and 0.08 doped samples were −90(1) K and −96(1) K. Previous work on β-$CrPO_4$ (Ref. 14) found values of $3.9\mu_B$ for the magnetic moment and −80 K for the Weiss temperature. The Neél temperatures estimated from the maxima in $d\chi/dT$ are 18.5(10) K and 19(1) K in the $x=0.02$ and 0.08 samples, respectively.

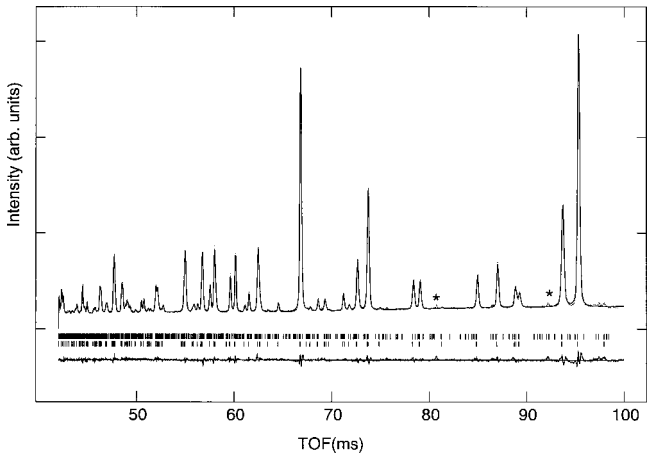

FIG. 7. Observed (dots), calculated and difference curves for $CrP_{0.96}V_{0.04}O_4$ at 2 K. The upper row of reflection markers indicate magnetic peaks, the lower row indicate nuclear peaks. Stars mark the positions of the most intense impurity peaks.

The susceptibility shows a broad maximum which has been interpreted[15] as characteristic of a Heisenberg antiferromagnetic linear chain (HALC). Using this model, the values of χ_{max} and T_{max} can be used to obtain estimates of the exchange constants in the system. The cusp in the susceptibility at around 20 K in the $x=0.02$ sample is similar to that reported for undoped $CrPO_4$, although this feature is much less evident in the $x=0.08$ sample. It has been interpreted[15] as the onset of three-dimensional magnetic order. For an $S=3/2$ chain[16] $2k_BT_{max}/|J|=4.75$ and $\chi_{max}|J|/2\,Ng^2\mu_B^2=0.091$, which can be used to estimate the intrachain exchange coupling. T_{max} gives $|J|=18$ K and $|J|=12$ K and χ_{max} gives $|J|=25.8$ K and $|J|=26.1$ K for the $x=0.02$ and 0.08 doped samples, respectively. The values obtained by Yamauchi and Ueda[15] were $|J|=19$ K and $|J|=24$ K from T_{max} and χ_{max}, respectively, for an undoped sample of β-$CrPO_4$. Hence the mean intrachain exchange constants in these compounds is $|J|\sim 20$ K.

The field cooled and zero-field cooled susceptibility data are shown on Fig. 9. For the $x=0.08$ sample there is a divergence of the two susceptibilities below 18 K. This is due to the freezing in of the disordered components of the magnetic moments which show a typical spin-glass behavior.

5. DISCUSSION

Samples of β-$CrP_{1-x}V_xO_4$ with $x=0-0.08$ have been studied using both neutron diffraction and magnetic susceptibility experiments. The Rietveld analysis of the neutron diffraction data give a detailed description of the crystal structures and their variation with x. Within the resolution of

TABLE II. Refined bond distances (Å) and angles (degrees) from the fits in Table I.

x	0.00	0.02	0.04	0.06	0.08
Cr-O(1)×2	1.9246(10)	1.9232(11)	1.9257(11)	1.9274(17)	1.9287(18)
Cr-O(2)×4	2.0298(6)	2.0290(7)	2.0281(8)	2.0290(12)	2.0277(13)
O(1)-Cr-O(1)	180.0	180.0	180.0	180.0	180.0
O(1)-Cr-O(2)×4	89.35(3)	89.38(3)	89.35(3)	89.28(5)	89.26(5)
O(1)-Cr-O(2)×4	90.64(3)	90.62(3)	90.65(3)	90.72(5)	90.74(5)
O(2)-Cr-O(2)×4	80.79(4)	80.78(5)	80.75(5)	80.81(8)	80.78(9)
O(2)-Cr-O(2)×2	99.21(4)	99.22(5)	99.25(5)	99.19(8)	99.22(9)
O(2)-Cr-O(2)×2	180.0	180.0	180.0	180.0	180.0
P/V-O(1)×2	1.503(1)	1.506(1)	1.504(1)	1.504(2)	1.504(2)
P/V-O(2)×2	1.572(1)	1.577(1)	1.582(2)	1.585(2)	1.590(2)
O(1)-P/V-O(1)	114.94(11)	114.73(12)	114.97(12)	115.28(19)	115.28(21)
O(1)-P/V-O(2)×4	108.52(3)	108.59(3)	108.54(3)	108.49(4)	108.48(5)
O(2)-P/V-O(2)	107.58(10)	107.52(11)	107.47(12)	107.32(18)	107.39(20)
Cr-O(2)-Cr	97.70(4)	97.72(5)	97.75(5)	97.69(8)	97.73(9)
Cr-O(1)-P/V	130.33(7)	130.41(7)	130.25(8)	130.03(11)	129.95(12)
Cr-O(2)-P/V×2	126.19(3)	126.15(3)	126.13(3)	126.13(5)	126.11(5)

the HRPD experiment, there is no variation of the propagation vector with temperature in the undoped sample. The value of $k_x = 0.3305(2)$ in the undoped sample is equivalent to a periodicity of $3.025(2)a_o$ which agrees with the value of $3.07(3)a_o$ obtained previously but is an order of magnitude more precise. Substitution of vanadate for phosphate increases the propagation vector linearly up to $x = 0.06$, where a maximum of $k_x = 0.3383(3)$ is reached. The ordered magnetic moment measured at 2 K is reduced by doping, showing an increasing localized disorder in the magnetic structure.

The variation of the magnetic propagation vector with chemical substitution evidences a subtle alteration of the exchange interactions in the structure. As the spins within each chain are antiferromagnetically ordered, the spiral order can be analyzed in terms of two exchange constants J_1 and J_2 in the xy plane as indicated on Fig. 1. J_1 is an antiferromagnetic coupling while J_2 is ferromagnetic. A commensurate magnetic structure with $k_x = 1/3$ requires $J_1 = -J_2$. The increase of k_x with x indicates that J_1 is increasing in magnitude relative to J_2 as vanadate is substituted for phosphate. The turn angle between the cation spins at (0,0,0) and (1/2,1/2,0) is $k_x\pi$ and this is related to the exchange constants by

$$\frac{J_2}{J_1} = -2\cos(k_x\pi).$$

The decrease of J_2/J_1 with x results from small changes in Cr-O-P/V-O-Cr superexchange pathways. The response of the metric tensor to vanadate substitution is anisotropic as x increases; $\Delta a/a = 0.42\%$, $\Delta b/b = 0.34\%$ and $\Delta c/c = -0.08\%$ for $x = 0$ to $x = 0.08$. It might be expected that the magnitude of the J_1 interaction should be reduced by a larger amount than the J_2 since the distance between chains in that direction increases by a marginally greater amount. Consideration of the crystal structure (Fig. 1) shows that J_1 is mediated by Cr-O (2)-P/V-O(2)-Cr linkages whereas J_2 goes through Cr-O(1)-P/V-O(2)-Cr. The variation of all the bond distances and angles is small except for the P-O(2) bond, which increases in length by ~0.02 Å as x increases from 0 to 0.08. This might be expected to have a stronger effect on the J_1 coupling than the J_2 as it occurs in the former pathway twice. If the increasing bond length is accompanied by a weakening of the superexchange interaction then $|J_2/J_1|$ should increase with x, whereas a decrease is observed. The phosphate and vanadate anions have different electronic

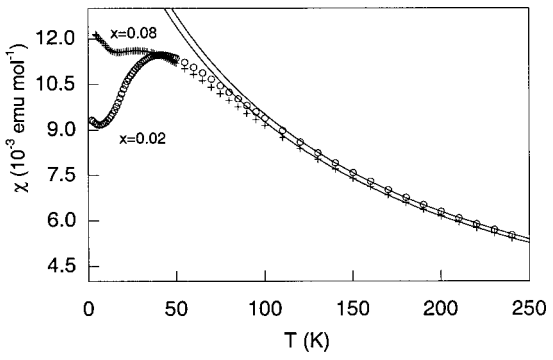

FIG. 8. Magnetic susceptibility data for the $x = 0.02$ and $x = 0.08$ $CrP_{1-x}V_xO_4$ samples with Curie Weiss fits.

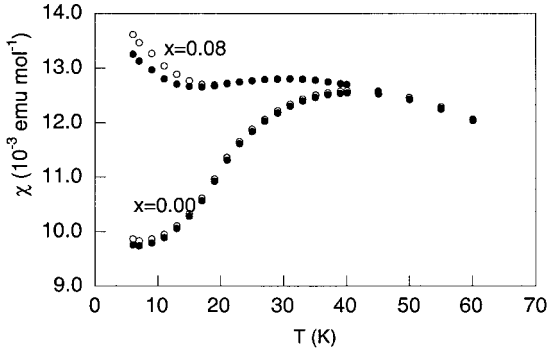

FIG. 9. Magnetic susceptibility data for $CrP_{1-x}V_xO_4$ for the $x = 0$ and $x = 0.08$ samples between 6 and 60 K. Open circles are for the field-cooled measurements, filled circles for zero-field cooled.

structures with the vanadate having vacant *d* states at significantly lower energy than the phosphate. This may be the dominant factor since the geometric arguments based on the changes in the average structure suggest an opposite trend for the propagation vector than that observed.

Although k_x decreases from the maximum value at $x=0.06$ to the $x=0.08$ sample, none of the refined structural or peak shape parameters follow the same trend. This may be related to some inhomogenieties as the $x=0.08$ sample is approaching the limit of the solid solubility. The steady reduction of the ordered moment with *x* indicates increasing localized disorder in the magnetic structure. The FWHM of the magnetic peaks is observed to increase with increasing *x*, which indicates progressively shorter magnetic correlation lengths within the sample as doping increases. The increasing anisotropy of the peak shape with *x* is evidenced by the refined coefficients of L_{ij}. A general increase in the Gaussian width of the peaks with *x* is also observed in the σ parameter, which describes the linear relationship between the FWHM and the TOF.

Given that this system does not exhibit a magnetic lock-in transition, it is notable that no temperature dependence of the magnetic propagation vector was found in the undoped sample. The thermal variation of the unit cell is much smaller than the variation with vanadate substitution; in addition, the thermal variation is more isotropic. These observations suggest that the variation J_2/J_1 with temperature is small compared to that for substitution. The outcome of a neutron diffraction experiment under high pressure would be of great interest to determine whether the variation of the propagation vector depends only upon the metric tensor of the crystal or also upon the electronic effects of a chemical substitution.[16]

The results of the susceptibility measurements indicate that the paramagnetic moment on the Cr^{3+} is largely unchanged by vanadate substitution, as would be expected. The susceptibility of the $x=0.02$ doped sample is similar to that of an undoped sample reported elsewhere,[14] although in the $x=0.08$ doped sample there is a suppression of the three-dimensional interchain magnetic order. The small difference in the Weiss constants between the samples indicates that the exchange interactions are altered slightly by substitution in keeping with the variation of k_x. The spin-glass behavior of the $x=0.08$ sample reflects local magnetic disorder effects arising from the vanadate substitution. The observation of spin-glass behavior and reduction of the ordered moment observed by neutron diffraction are all consistent with increasing magnetic frustration with *x*.

In conclusion, the magnetic structure of β-$CrPO_4$ is not locked into a commensurate $3\times1\times1$ supercell and a coincidental balance of superexchange interactions leads to the value of $k_x\approx1/3$. The lack of single-ion anistropic effects is in keeping with the spin only behavior of Cr^{3+}. Substitution of vanadate for phosphate leads to a slight increase in the magnetic propagation vector k_x and induces a spin-glass component in the static magnetic order.

ACKNOWLEDGMENTS

We thank Dr. Richard Ibberson, Miss J. A. McAllister, and Mr. J. van Duijn for assistance with data collection and EPSRC for provision of neutron beam time. J.P.W. acknowledges EPSRC and the Rutherford Appleton Laboratory for financial support.

[1] J. P. Attfield, P. D. Battle, and A. K. Cheetham, J. Solid State Chem. **57**, 357 (1985).
[2] J. P. Attfield, D. Phil. thesis, University of Oxford, 1987.
[3] G. Will, B. C. Frazer, G. Shirane, D. E. Cox, and P. J. Brown, Phys. Rev. **140**, A2139 (1965).
[4] J. Solyom, Physica (Amsterdam) **32**, 1243 (1966).
[5] M. Lecomte, J. de Gunzbourg, M. Teyrol, A. Miedan-Gros, and Y. Allain, Solid State Commun. **10**, 235 (1972); E. Legrand, S. Hautecler, and G. Will, J. Magn. Magn. Mater. **15**, 529 (1980).
[6] B. C. Frazer and P. J. Brown, Phys. Rev. **125**, 1283 (1962).
[7] R. Glaum, M. Reehuis, N. Stußer, U. Kaiser, and F. Reinauer, J. Solid State Chem. **126**, 15 (1996).
[8] R. A. Cowley, D. A. Jehan, D. F. McMorrow, and G. J. McIntyre, Phys. Rev. Lett. **66**, 1521 (1991).
[9] J. B. Forsyth, J. P. Wright, M. Marcos, J. P. Attfield, and C. Wilkinson, J. Phys.: Condens. Matter **11**, 1473 (1999).
[10] J. P. Attfield, A. W. Sleight, and A. K. Cheetham, Nature (London) **322**, 620 (1986).
[11] A. C. Larson and R. B. VonDreele, Los Alamos National Laboratory Report No. LA-UR-86-748 (unpublished).
[12] J. B. Forsyth, TF112M, 1999; J. C. Matthewman, P. Thompson, and P. J. Brown, J. Appl. Crystallogr. **15**, 167 (1982).
[13] R. B. Von Dreele and C. M. B. Line (unpublished).
[14] N. Kinomura, F. Muto, and M. Koizumi, J. Solid State Chem. **45**, 252 (1982).
[15] T. Yamauchi and Y. Ueda, J. Magn. Magn. Mater. **177**, 705 (1998).
[16] R. L. Carlin, *Magnetochemistry* (Springer, Berlin, 1986).